Supporting Information

On the support dependency for the CO_2 methanation - Decoupling size and support effects

Dr.-Ing. Jan Ilsemann[1,*], PD Dr. Mangir M. Murshed[2, 3], Prof. Dr. Thorsten M. Gesing[2, 3], Prof. Dr. Jan Kopyscinski[4] and Prof. Dr. Marcus Bäumer[1,3]

[1] University of Bremen, Institute of Applied and Physical Chemistry, 28359 Bremen, Germany

[2] University of Bremen, Institute of Inorganic Chemistry and Crystallography, 28359 Bremen, Germany

[3] University of Bremen, MAPEX Center for Materials and Processes, 28359 Bremen, Germany

[4] McGill University, Catalytic Process Engineering, Montreal, QC H3A 0C5, Canada

* Corresponding author (E-Mail: jan.ilsemann@uni-bremen.de)

Additional characterizations

1. X-ray powder diffraction

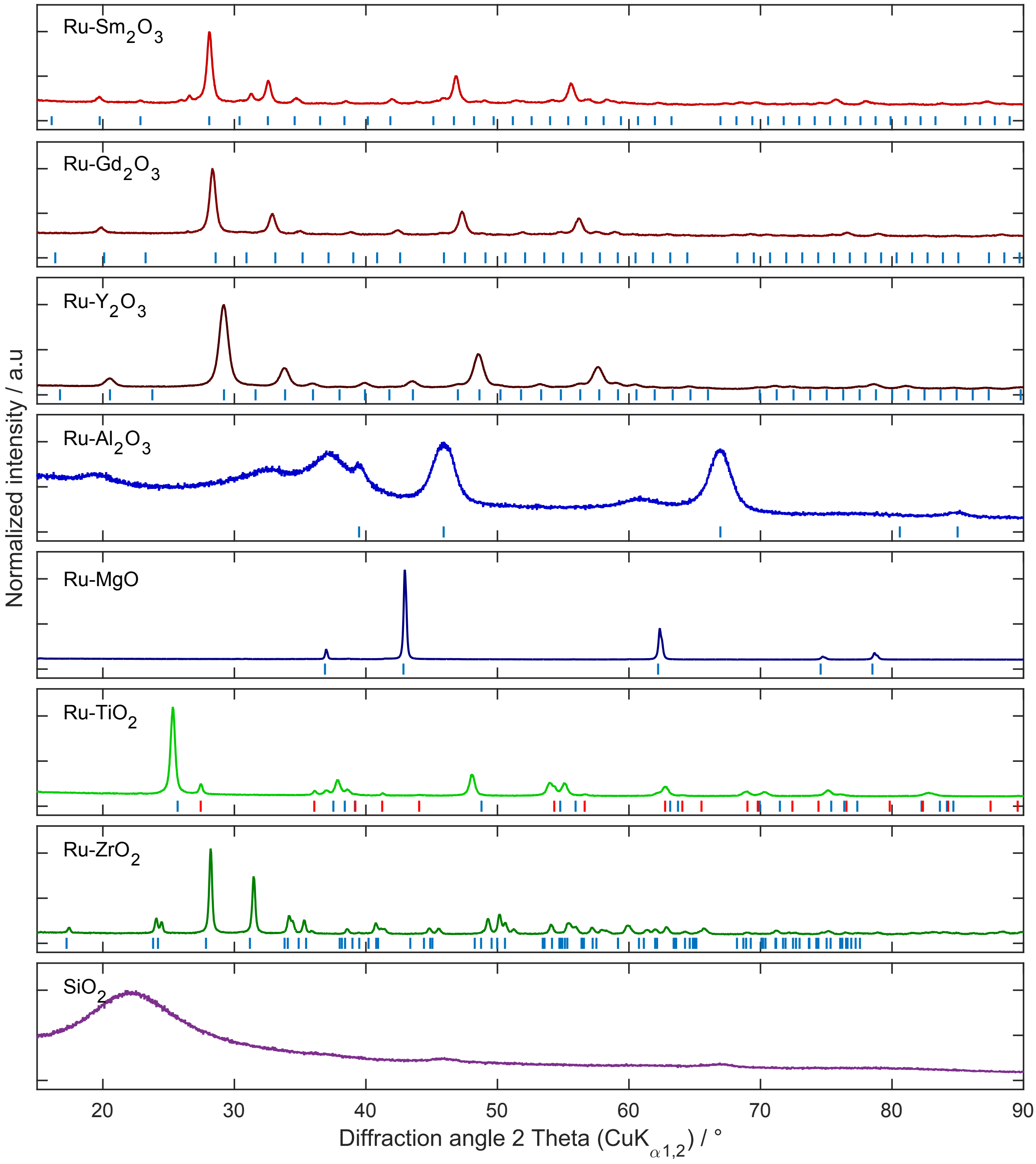

Figure S1: X-ray powder diffraction patterns of the investigated catalysts. The tick marks indicate the possible Bragg reflections of the respective oxide phases. Sm_2O_3, Gd_2O_3 and Y_2O_3 - $Ia\bar{3}$;[1] γ-Al_2O_3 - $Fm\bar{3}m$;[2] MgO - $Fm\bar{3}m$;[3] TiO_2 – P 4_2/mnm (red) and I 4_1/amd (blue);[4, 5] ZrO_2 - P12_1/c1.[6]

2. N_2 physisorption

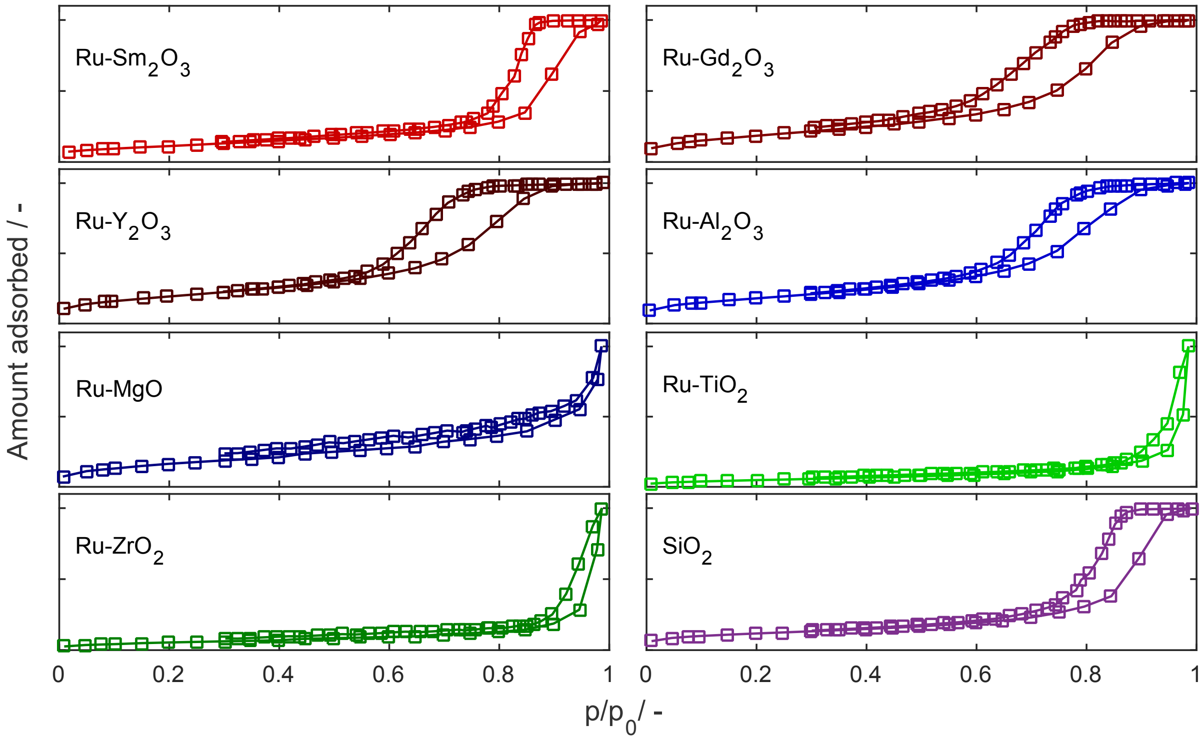

Figure S2: N_2 physisorption isotherms of the investigated catalysts.

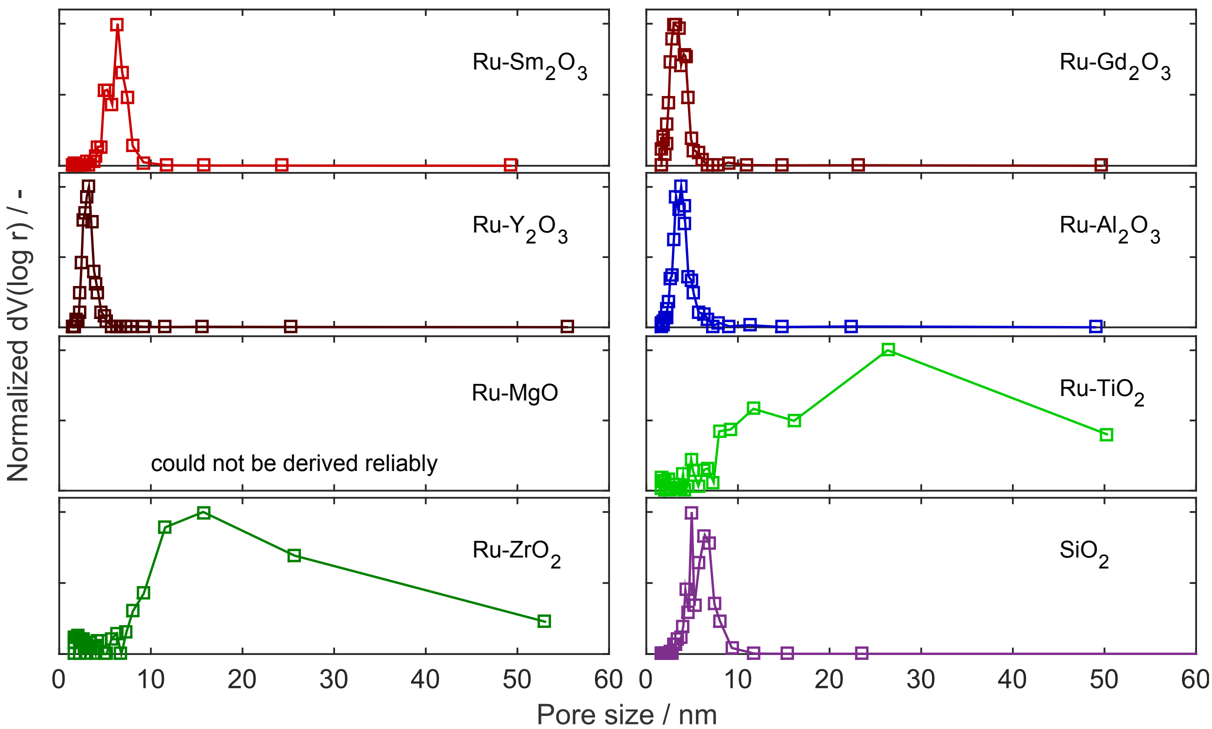

Figure S3: Derived pore-size distributions using the BJH model (applied to the desorption branch of the isotherm) of the investigated catalysts.

Additional catalytic data

1. Measured outlet concentrations

Table S1 Measured outlet volume concentrations of CO, CH_4 and CO_2

	CO / vol.%	CH_4 / vol.%	CO_2 / vol.%
200 °C			
Ru-Sm_2O_3	0	0	9.73
Ru-Gd_2O_3	0	0.01	9.76
Ru-Y_2O_3	0	0	9.73
Ru-TiO_2	0	0.13	9.66
Ru-ZrO_2	0	0.02	9.78
Ru-Al_2O_3	0	0.03	9.74
Ru-SiO_2	0	0	9.76
230 °C			
Ru-Sm_2O_3	0	0.07	9.71
Ru-Gd_2O_3	0	0.08	9.73
Ru-Y_2O_3	0	0.04	9.71
Ru-TiO_2	0	0.38	9.54
Ru-ZrO_2	0	0.10	9.73
Ru-Al_2O_3	0	0.10	9.68
Ru-SiO_2	0	0	9.76
270 °C			
Ru-Sm_2O_3	0.05	0.42	9.48
Ru-Gd_2O_3	0.04	0.47	9.52
Ru-Y_2O_3	0.03	0.25	9.58
Ru-TiO_2	0	1.18	9.14
Ru-ZrO_2	0	0.54	9.52
Ru-Al_2O_3	0.02	0.40	9.51
Ru-SiO_2	0.05	0.07	9.68
290 °C			
Ru-Sm_2O_3	0.09	0.98	9.17
Ru-Gd_2O_3	0.07	1.06	9.20
Ru-Y_2O_3	0.07	0.59	9.38
Ru-TiO_2	0	1.90	8.78
Ru-ZrO_2	0.01	1.2	9.4
Ru-Al_2O_3	0.05	0.76	9.33
Ru-SiO_2	0.14	0.18	9.54
310 °C			
Ru-Sm_2O_3	0.19	2.67	8.29
Ru-Gd_2O_3	0.13	2.30	8.54
Ru-Y_2O_3	0.12	1.34	8.97
Ru-TiO_2	0.02	2.87	8.30
Ru-ZrO_2	0.02	2.09	8.88
Ru-Al_2O_3	0.11	1.35	8.99
Ru-SiO_2	0.31	0.36	9.27
350 °C			
Ru-Sm_2O_3	0.33	7.20	5.92
Ru-Gd_2O_3	0.30	7.25	5.99
Ru-Y_2O_3	0.30	5.74	6.69
Ru-TiO_2	0.08	5.45	7.02
Ru-ZrO_2	0.08	4.43	7.95
Ru-Al_2O_3	0.36	3.34	7.82
Ru-SiO_2	1.03	1.15	8.27
400 °C			

Ru-Sm_2O_3	0.42	8.47	5.28
Ru-Gd_2O_3	0.39	9.78	4.73
Ru-Y_2O_3	0.35	9.94	4.62
Ru-TiO_2	0.26	8.44	5.42
Ru-ZrO_2	0.31	6.32	6.91
Ru-Al_2O_3	0.82	6.29	6.03
Ru-SiO_2	1.78	3.49	6.56

2. CO_2 consumption rates and CH_4 selectivity

We define the conversion and methane selectivity as

$$r_{CO_2} = \frac{\dot{n}_{CO_2,in} - \dot{n}_{CO_2,out}}{m_{Ru}}$$

$$S_{CH_4} = \frac{r_{CH_4}}{r_{CO_2}}.$$

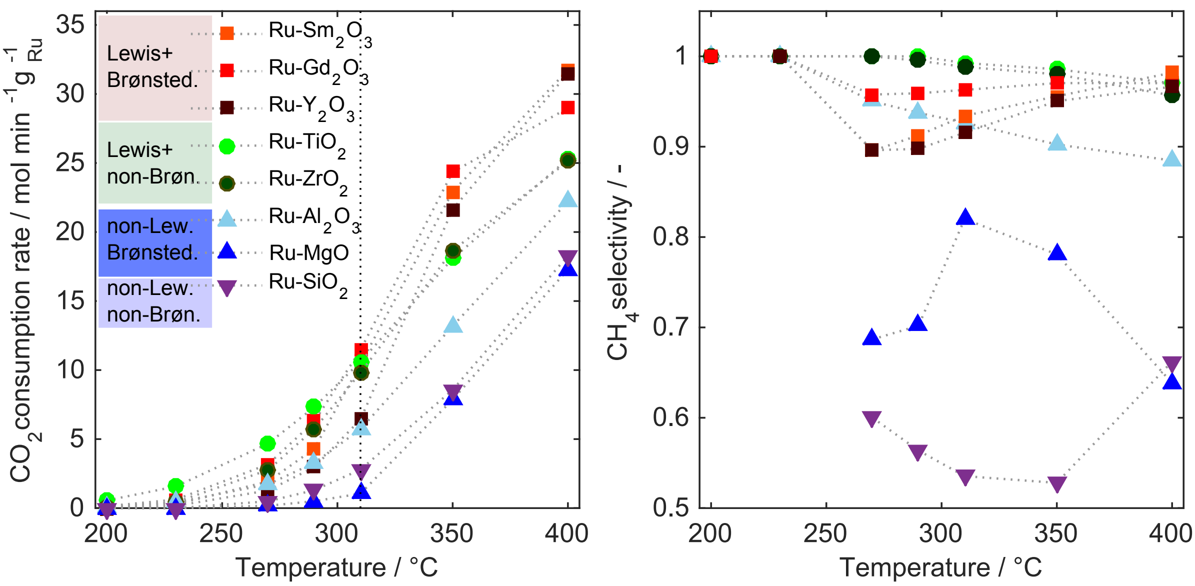

Figure S4 (left) CO_2 conversion rates and (right) CH_4 selectivities for all cataysts in the investigated temperature range. Reaction conditions: pressure 1 bar, flow rate 50 mL min^{-1}, 4/1/5 $H_2/CO_2/Ar$, 50 mg catalyst. The vertical line at 310°C indicates a change regarding the best performing catalysts.

3. Weisz-Prater calculations

The criterion was calculated for all temperatures and catalysts according to the following equation

$$WP = \frac{r^{eff}\rho_{cat}d_{cat}^{2}}{4c_{CO_2}D_{CO_2}^{eff}} < 1$$

Knudsen diffusion is taken into account for all catalysts except Ru-TiO_2 and Ru-ZrO_2 as these catalysts exhibit macropores. The following catalyst densities are assumed (as stated by the supplier, if available): $\rho_{Al2O3} = 2.3\cdot10^6$ g m^{-3}, $\rho_{MgO} = 3.6\cdot10^6$ g m^{-3}, $\rho_{TiO2} = 4.2\cdot10^6$ g m^{-3}, $\rho_{ZrO2} = 5.7\cdot10^6$ g m^{-3} and $\rho_{SiO2} = 2.7\cdot10^6$ g m^{-3}. For the REO catalysts, the densities were approximated as $\rho_{Sm2O3} = 6.9\cdot10^6$ g m^{-3}, $\rho_{Gd2O3} = 7.4\cdot10^6$ g m^{-3} and $\rho_{Y2O3} = 6.9\cdot10^6$ g m^{-3}. For the xerogel catalysts a tortuosity of 2 was assumed based on a previous study on rare earth metal oxide aerogels.[9] For all other catalysts, the tortuosity was presumed to be 3. The results are compiled below.

Table S2 Results of Weisz-Prater criterion calculations.

	200 °C	230 °C	270 °C	290 °C	310 °C	350 °C	400 °C
Ru-Sm_2O_3	0	0.0092	0.0561	0.1185	0.2724	0.5420	0.6683
Ru-Gd_2O_3	0.0054	0.0217	0.0992	0.1854	0.3209	0.6174	0.6542
Ru-Y_2O_3	0	0.0039	0.0270	0.0593	0.1214	0.3709	0.4804
Ru-Al_2O_3	0.0028	0.0091	0.0347	0.0623	0.1037	0.2179	0.3294
Ru-MgO	0	0	0.0054	0.0150	0.0299	0.2034	0.4013
Ru-TiO_2	0.0229	0.0589	0.1564	0.2315	0.3184	0.4912	0.6123
Ru-ZrO_2	0.0030	0.0175	0.0998	0.1954	0.3173	0.5468	0.6554
Ru-SiO_2	0	0	0.0116	0.0292	0.0593	0.1661	0.3184

4. Arrhenius plot

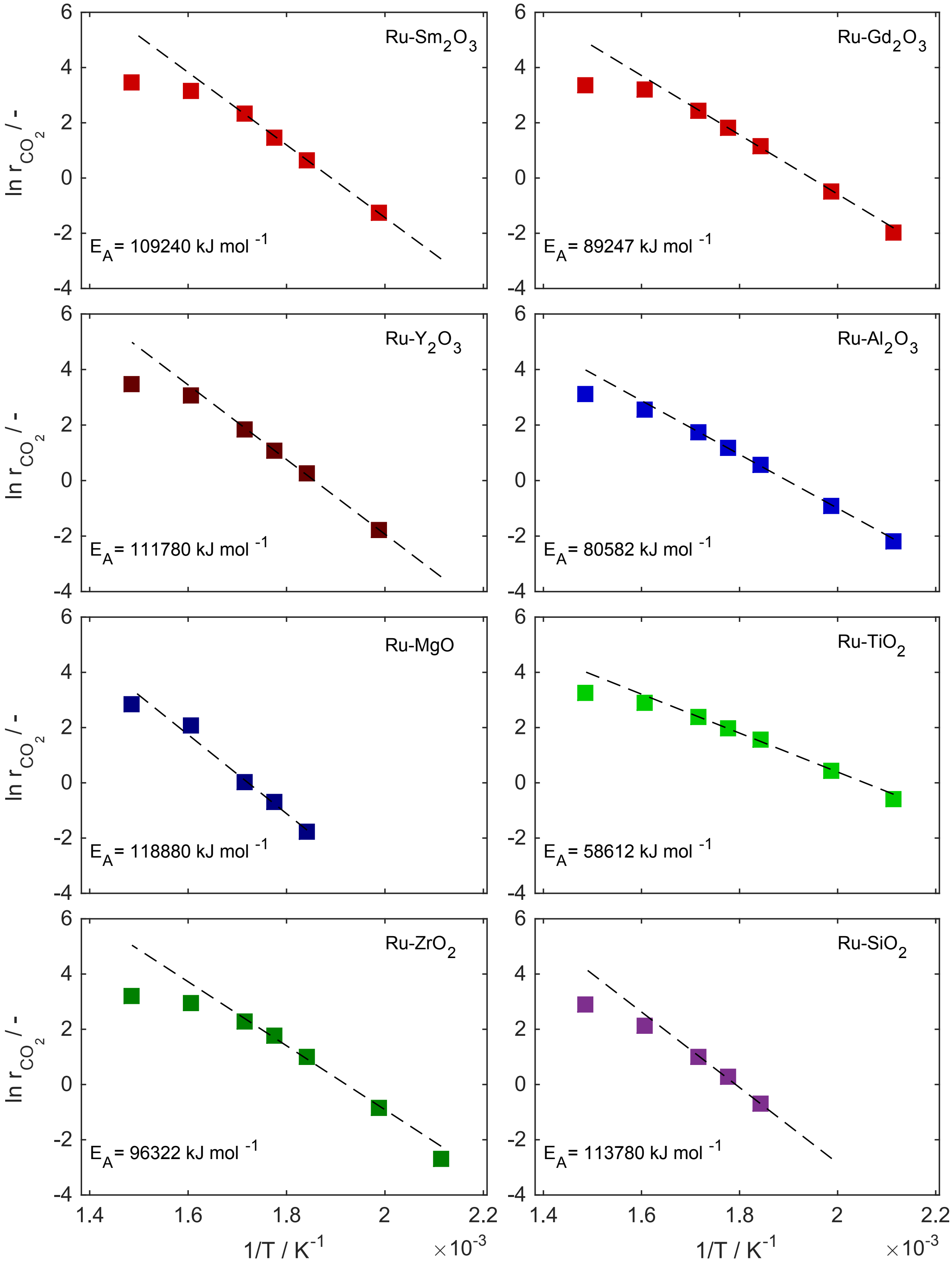

Figure S5: Arrhenius presentation of all catalysts for the investigated temperatures. The dashed line refers to a linear fit in the temperature range 200-310 °C, showing the deviation at elevated temperatures.

5. *Stability runs*

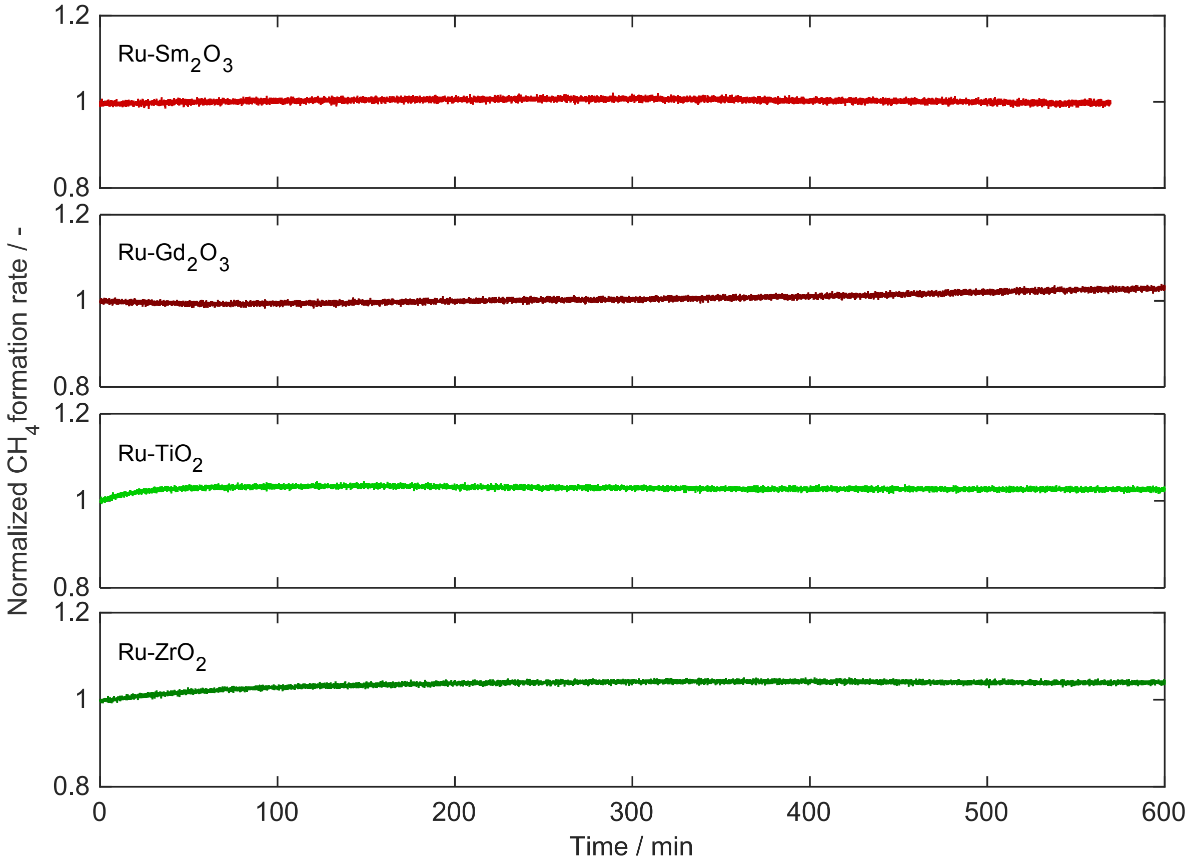

Figure S6: Normalized methane formation rate vs. time at 400 °C for selected catalysts. The methane formation rate was chosen as a descriptor as it would reflect changes in the conversion rate as well as selectivity. The rates are normalized to the initial methane formation rate. Reaction conditions: pressure 1 bar, flow rate 50 mL min^{-1}, 4/1/5 H_2/CO_2/Ar, 50 mg catalyst

6. TEM images of selected, spent catalysts

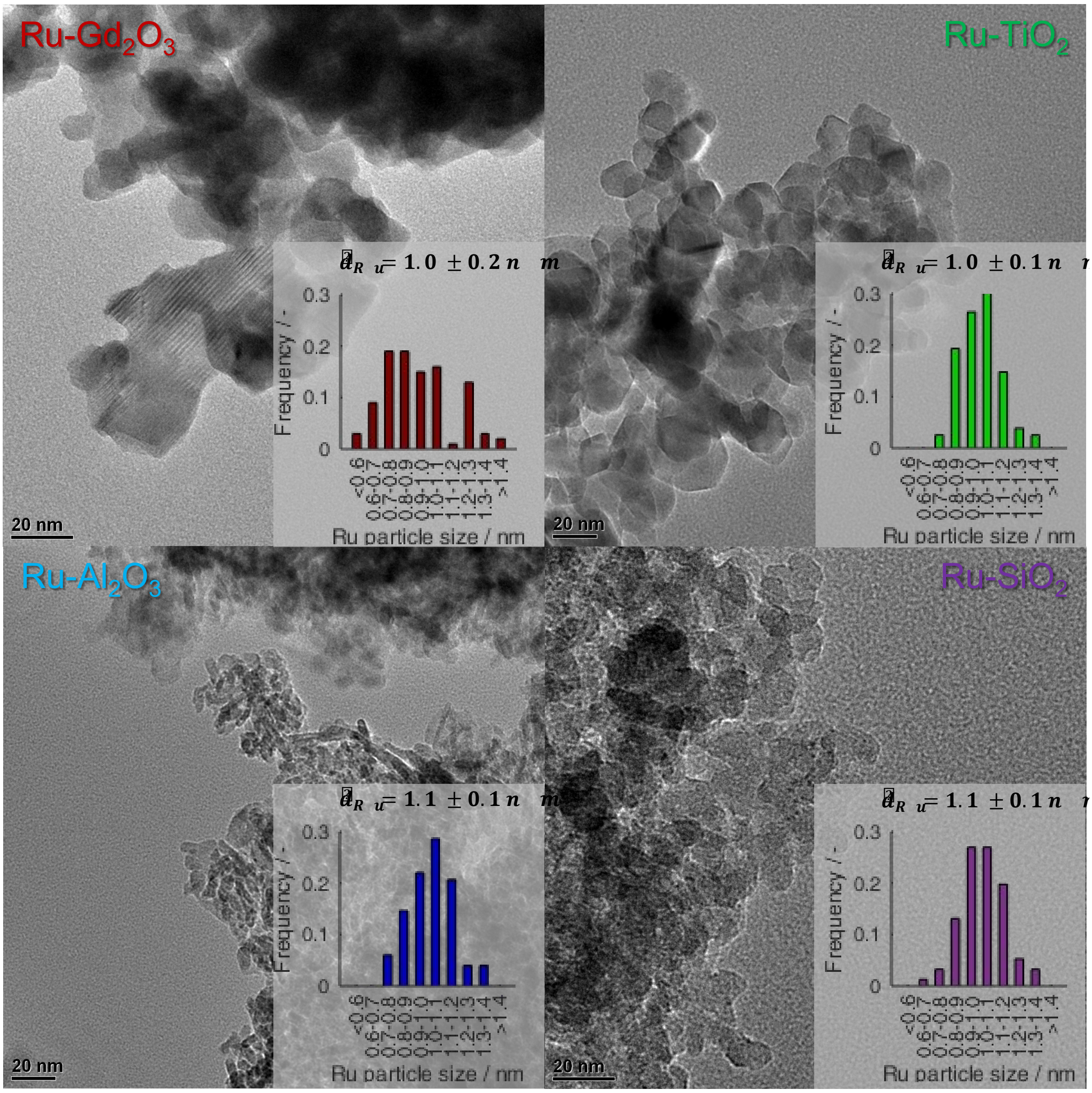

Figure S7: TEM images of the catalysts after reaction.

7. Reproducibility

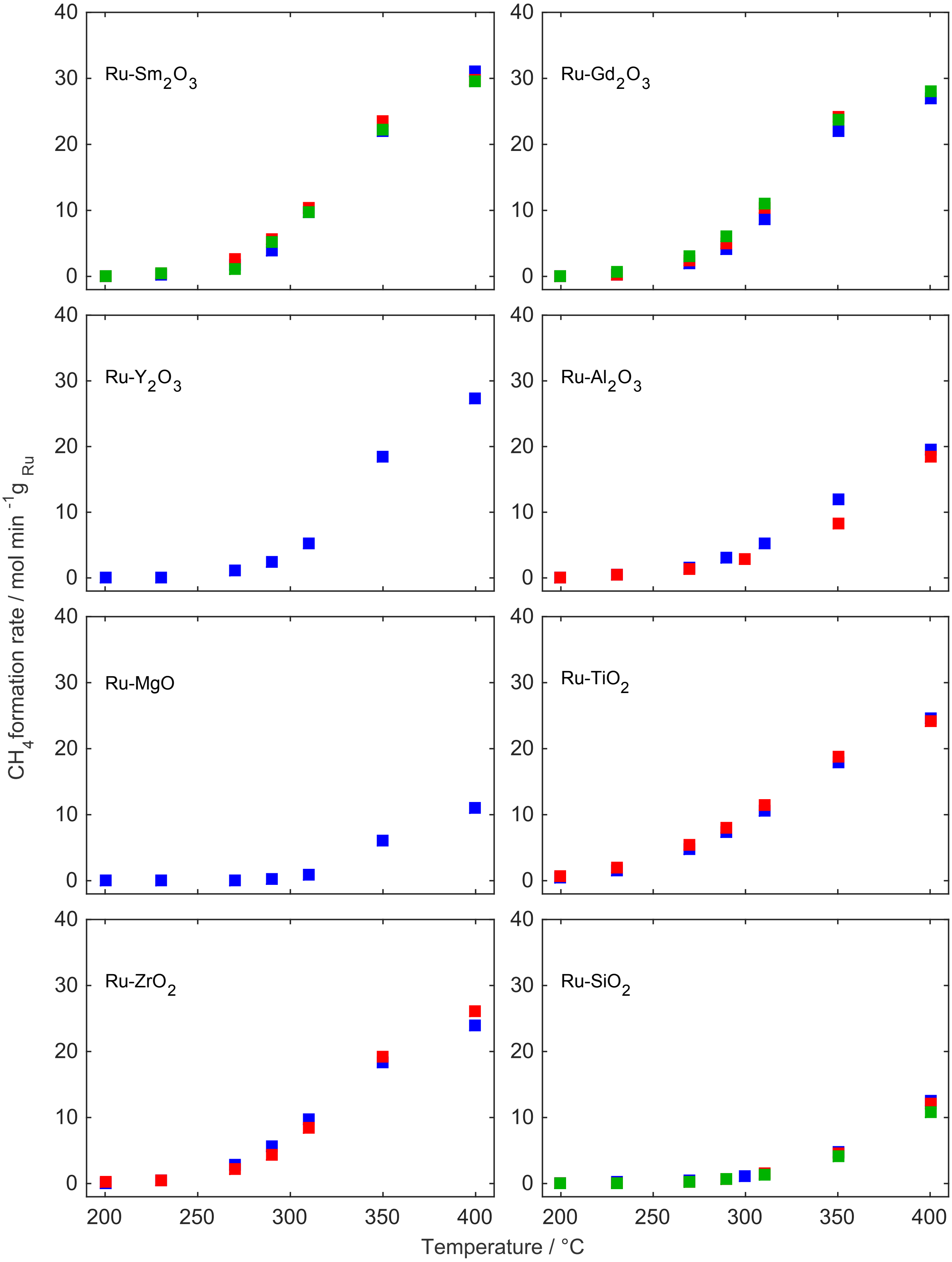

Figure S8: Methane formation rates for the investigated catalysts and for various catalyst batches to ensure reproducibility of the synthesis route; blue symbols indicate catalyst batch 1, red symbols indicate batch 2, green symbols indicate batch 3. Another batch refers to newly synthesized Ru nanoparticles and support materials (if synthesized in-house). The methane formation rate was chosen as a descriptor as it would reflect changes in the conversion rate as well as selectivity. In the main manuscript data corresponding to batch 1 is shown.

Additional DRIFTS results

1. *Deconvoluted and fitted DRIFT spectra, exemplary shown for Ru-Gd_2O_3 at 160 °C (spectra acquired during the temperature dependent reaction study, Fig. 6 in the main manuscript)*

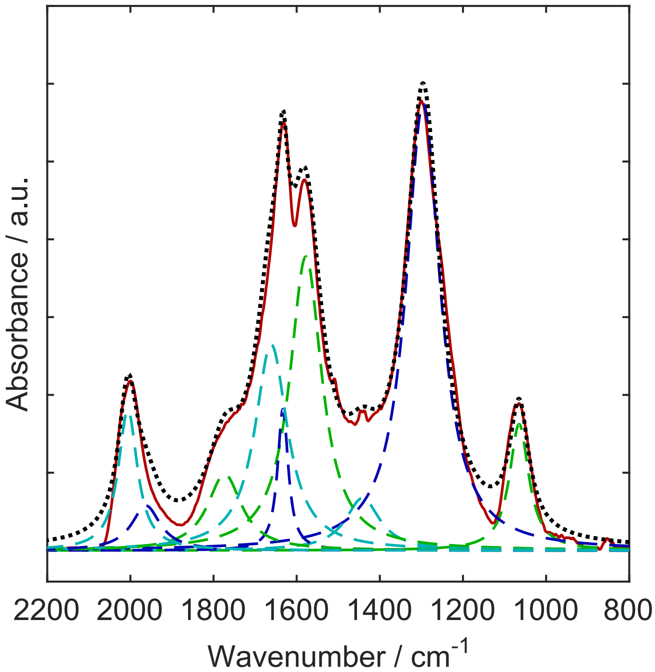

Figure S9: DRIFTS – reaction study on Ru-Gd_2O_3 at 160 °C, 5 vol.% CO_2, 20 vol.% H_2 in He, $\dot{V}_{tot}$= 100 mL min^{-1}. Solid red line: measured spectra, dashed green/blue lines: fitted peaks, dotted black line: calculated spectra based on the fitted peaks. The peaks were fitted using the Gauss-Lorentzian model.

2. *Temperature-dependent DRIFTS-reaction study on Ru-Sm_2O_3*

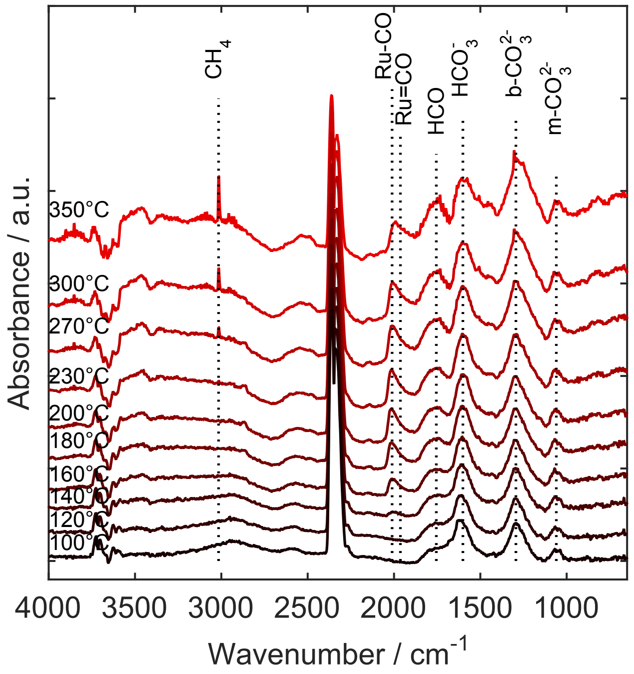

Figure S10: Temperature-dependent DRIFTS – reaction study on Ru-Sm_2O_3, 5 vol.% CO_2, 20 vol.% H_2 in He, $\dot{V}_{tot}$= 100 mL min^{-1} references: [10–16]. The spectra qualitatively match the results on the Ru-Gd_2O_3 catalyst.

3. Additional DRIFTS results on Ru-Al_2O_3, Ru-MgO and Ru-SiO_2

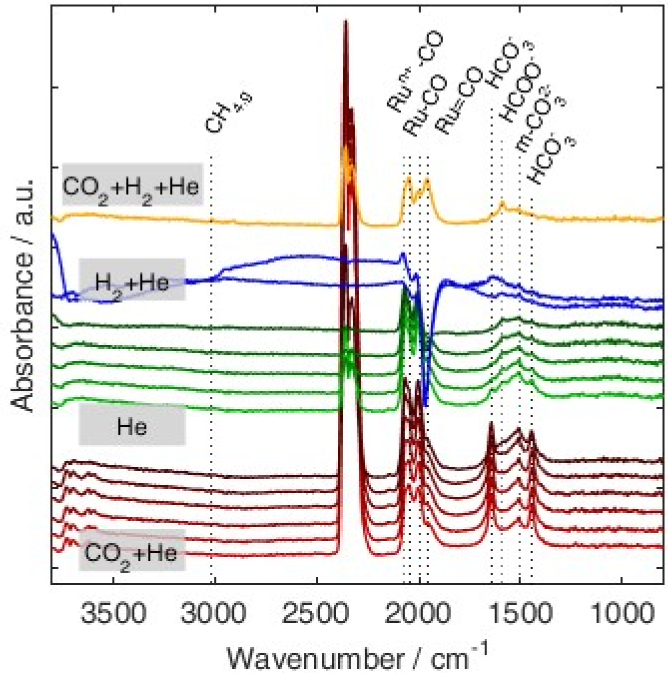

Figure S12: Isothermal DRIFTS experiments carried out for Ru-Al_2O_3 at 350 °C under different gas atmospheres. Red spectra: exposure to 5 vol.% CO_2 in He for 15 min; blue spectra: pure He for 20 min; green spectra: subsequent exposure to 20 vol.% H_2 in He; yellow trace: exposure to 5 vol.% CO_2 and 20 vol.% H_2 in He, $\dot{V}_{tot} = 100\ mL\ min^{-1}$. Temporal evolution of the spectra from lighter to darker colors (bottom to top).

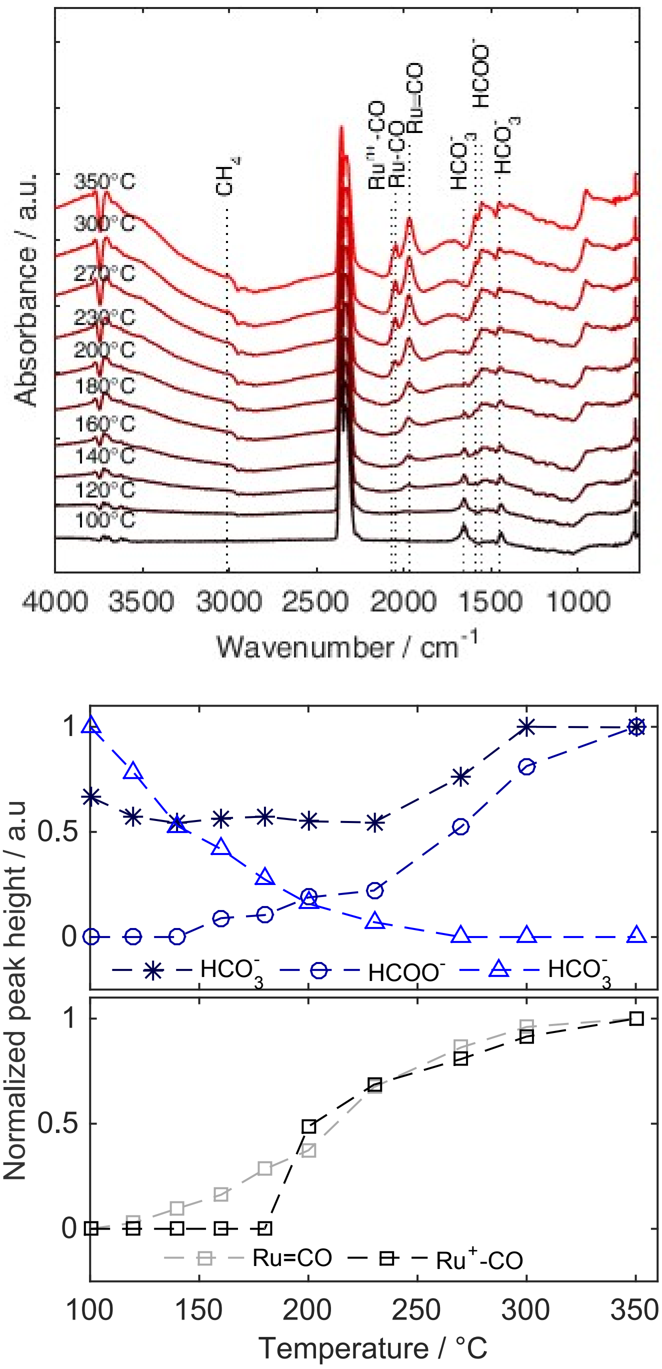

Figure S13: (top) Temperature-dependent DRIFTS – reaction study on Ru-Al_2O_3, (bottom) normalized peak height for HCO_3^- (1441 cm^{-1}), $HCOO^-$ (1587 cm^{-1}), Ru=CO (1971 cm^{-1}), Ru-CO (2046 cm^{-1}) and Ru^+-CO (2069 cm^{-1}); conditions: 5% CO_2, 20% H_2 in He, $\dot{V}_{tot} = 100\ mL\ min^{-1}$;references: [10, 17, 18]

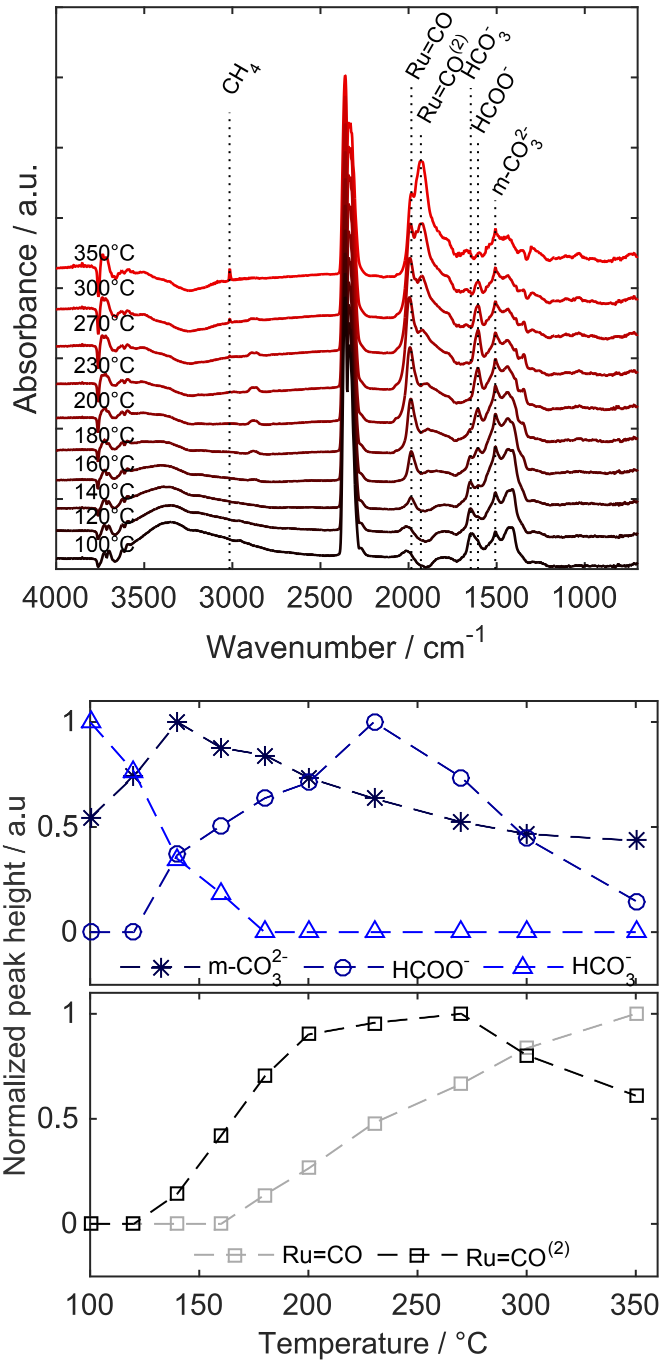

Figure S14: (top) Temperature-dependent DRIFTS – reaction study on Ru-MgO, (bottom) normalized peak height for m-CO_3^{2-} (1508 cm^{-1}), $HCOO^-$ (1606 cm^{-1}), HCO_3^- (1647 cm^{-1}), Ru=CO (1930 cm^{-1}) and Ru=CO$^{(2)}$ (1984 cm^{-1}); conditions: 5 vol.% CO_2, 20 vol.% H_2 in He, $\dot{V}_{tot} = 100\ mL\ min^{-1}$*.; references:* [19–21]

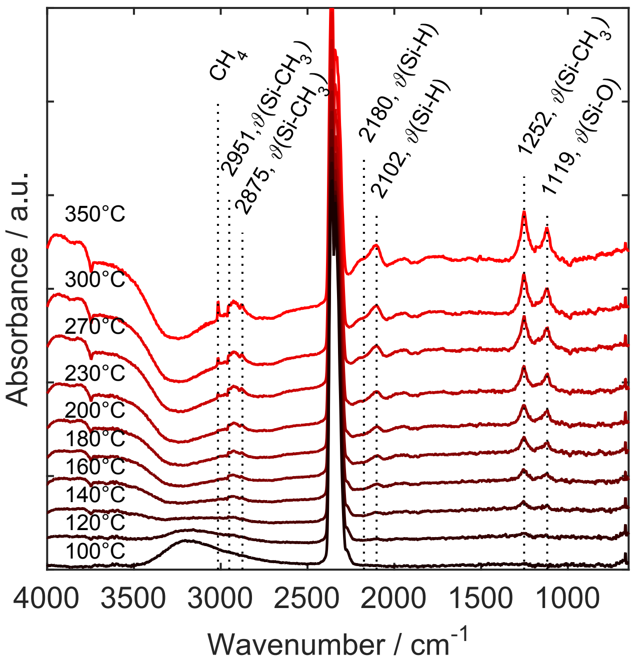

Figure S15: Temperature-dependent DRIFTS – reaction study on Ru-SiO$_2$, 5 vol.% CO$_2$, 20 vol.%H$_2$ in He, $\dot{V}_{tot}$= 100 mL min^{-1}; references: [22–24]

Raman results

1. *Experimental description*

Raman spectra were recorded on a LabRam ARAMIS (Horiba Jobin Yvon) Micro-Raman spectrometer equipped with a laser working at 785 nm and less than 20 mW. The use of a 50x long working distance objective (Olympus) with a numerical aperture of 0.55 provides a focus spot of about 5 µm diameter when closing the confocal hole to 1000 µm. The spectra were collected in the range 90 cm^{-1} to 800 cm^{-1} with a spectral resolution of approximately 1.2 cm^{-1} using a grating of 1800 grooves mm^{-1} and a thermoelectrically cooled CCD detector (Synapse, 1024 x 256 pixels). The spectral positions were calibrated against the Raman mode of Si before and after the sample measurements. In some cases, the optimized filtering was required to minimize the fluorescence and to reduce laser intensity to avoid sample damage. At least 15 spectra were collected with an acquisition time of 10 s /window for an adequate signal-to-noise ratio. The high-temperature spectra were performed using a Linkam heating stage (TS1500) connected to a continuous gas (5 vol.% H$_2$ + 95 vol.% Ar) supply to the stage. The powder samples were loaded and the compartment was flushed with the gas mixture for several minutes before heating at the sample 50 °C. Afterward, the temperature was ramped to 200 °C at 20 °C/min and kept for 45 min. In each case, the sample was then cooled down from the target temperature to 50 °C followed by collecting spectra to exclude the quasiharmonic (lattice thermal expansion effects) and anharmonic contributions in shifting the Raman bands. After a thermal equilibration period of 5 min spectra were collected, and the experiment was repeated between 50 °C and 400 °C with a 50 °C step (e.g., 50 °C -> 200 °C -> 50 °C -> 250 °C-> 50 °C -> 300 °C -> 50 °C -> 350 °C -> 50°C ->400 °C -> 50 °C). As much as three different locations were chosen at each temperature step, and an averaged spectrum was produced for a better statistics. After background correction and normalization, the peaks were fitted with Gauss-Lorentzian model.

2. Raman spectra of the as-prepared catalysts

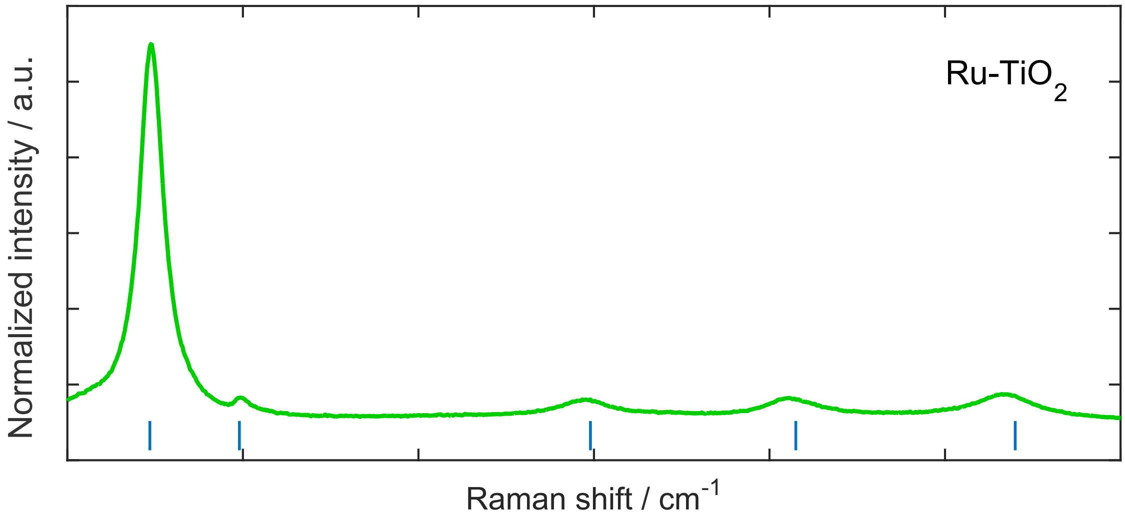

Figure S16: Raman spectra of the as-prepared Ru-TiO_2 catalyst at ambient condition. The tick marks refer to observed band positions of anatase.[7]

3. Temperature-dependent shift of the Raman frequency

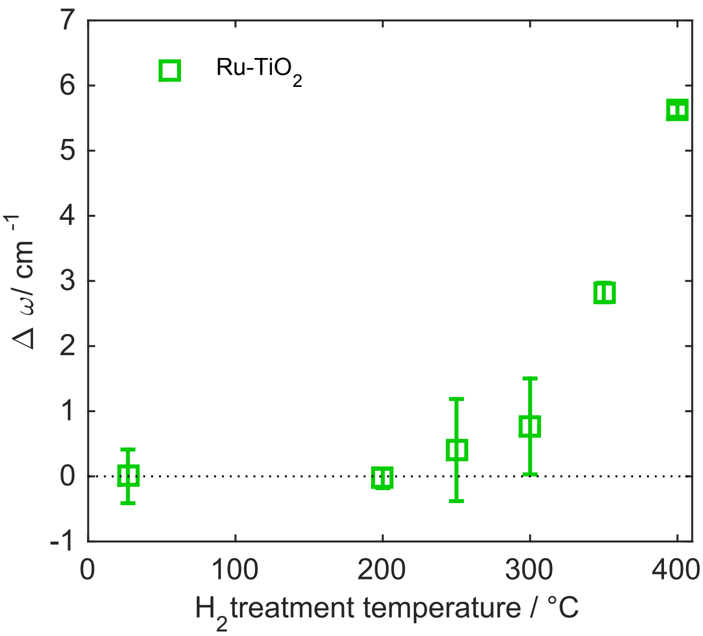

Figure S17: Temperature-dependent changes of Raman frequencies (Δω) of Ru-TiO_2 (147 cm^{-1}) under H_2 atmosphere.

References Supporting Information

1 Worsley, M.A., J. Ilsemann, T.M. Gesing, V. Zielasek, A.J. Nelson, R.A.S. Ferreira, L.D. Carlos, A.E. Gash, and M. Bäumer, *J. Sol-Gel Sci. Technol.*, 2019, **89**, 176–188.

2 Smrčok, Ľ., V. Langer, and J. Křesťan, *Acta Crystallogr. Sect. C Cryst. Struct. Commun.*, 2006, **62**, 83–84.

3 Bernuy-Lopez, C., M. Allix, C.A. Bridges, J.B. Claridge, and M.J. Rosseinsky, *Chem. Mater.*, 2007, **19**, 1035–1043.

4 Baur, W.H., *Acta Crystallogr.*, 1956, **9**, 515–520.

5 Weirich, T.E., M. Winterer, S. Seifried, and J. Mayer, *Acta Crystallogr. Sect. A Found. Crystallogr.*, 2002, **58**, 308–315.

6 Whittle, K.R., G.R. Lumpkin, and S.E. Ashbrook, *J. Solid State Chem.*, 2006, **179**, 512–521.

7 Wajid Shah, M., Y. Zhu, X. Fan, J. Zhao, Y. Li, S. Asim, and C. Wang, *Sci. Rep.*, 2015, **5**, 15804.

8 Eder, D. and R. Kramer, *Phys. Chem. Chem. Phys.*, 2002, **4**, 795–801.

9 Mueller, R., S. Zhang, M. Klink, M. Bäumer, and S. Vasenkov, *Phys. Chem. Chem. Phys.*, 2015, **17**, 27481–27487.

10 Eckle, S., H.-G. Anfang, and R.J. Behm, *J. Phys. Chem. C*, 2011, **115**, 1361–1367.

11 Daturi, M., C. Binet, J.C. Lavalley, and G. Blanchard, *Surf. Interface Anal.*, 2000, **30**, 273–277.

12 Dreyer, J.A., P. Li, L. Zhang, G. Khai Beh, R. Zhang, P. H-L Sit, and W. Yang Teoh, *Appl. Catal. B Environ.*, 2017, **219**, 715–726.

13 Wang, X., H. Shi, J.H. Kwak, and J. Szanyi, *ACS Catal.*, 2015, **5**, 6337–6349.

14 Aldana, P.A.U., F. Ocampo, K. Kobl, B. Louis, F. Thibault-Starzyk, M. Daturi, P. Bazin, S. Thomas, and A.C. Roger, *Catal. Today*, 2013, **215**, 201–207.

15 Baidya, T. and P. Bera, *Catal. Struct. React.*, 2015, **1**, 110–119.

16 Mitchell, W.J., Y. Wang, J. Xie, and W.H. Weinberg, *J. Am. Chem. Soc.*, 1993, **115**, 4381–4382.

17 Denkwitz, Y., A. Karpenko, V. Plzak, R. Leppelt, B. Schumacher, and R.J. Behm, *J. Catal.*, 2007, **246**, 74–90.

18 Wang, X., Y. Hong, H. Shi, and J. Szanyi, *J. Catal.*, 2016, **343**, 185–195.

19 Cornu, D., H. Guesmi, J.M. Krafft, and H. Lauron-Pernot, *J. Phys. Chem. C*, 2012, **116**, 6645–6654.

20 Schweicher, J., A. Bundhoo, A. Frennet, N. Kruse, H. Daly, and F.C. Meunier, *J. Phys. Chem. C*, 2010, **114**, 2248–2255.

21 Kwon, H. and D.G. Park, *Bull. Korean Chem. Soc.*, 2009, **30**, 2567–2573.

22 Oh, T. and C.K. Choi, *J. Korean Phys. Soc.*, 2010, **56**, 1150–1155.

23 Kopani, M., M. Mikula, D. Kosnac, J. Gregus, and E. Pincik, *J. Electr. Eng.*, 2017, **68**, 53–57.

24 Wang, Z.H., T. Urisu, H. Watanabe, K. Ooi, G. Ranga Rao, S. Nanbu, J. Maki, and M. Aoyagi, *Surf. Sci.*, 2005, **575**, 330–342.